



Supplement of

**Thermodynamic and cloud evolution in
a cold-air outbreak during HALO-(AC)³:
quasi-Lagrangian observations compared
to the ERA5 and CARRA reanalyses**

Benjamin Kirbus et al.

Correspondence to: Benjamin Kirbus (benjamin.kirbus@uni-leipzig.de) and Manfred Wendisch (m.wendisch@uni-leipzig.de)

The copyright of individual parts of the supplement might differ from the article licence.

Supplemental material

Calculation of time over ice-free oceans for HALO and Polar 6

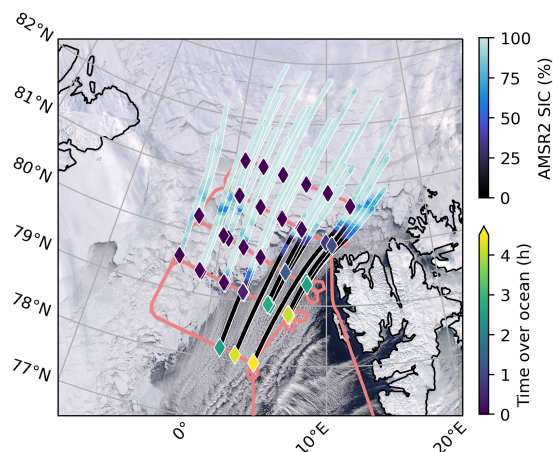


Figure S1. Procedure of calculating the time over ice-free ocean for HALO. Air masses are started at 10 hPa above ground for all released dropsonde locations. Trajectories are then calculated 12h backwards and the AMSR2 sea-ice concentration (SIC; Ludwig et al., 2020) traced. Time is integrated backwards as long as the SIC is below 20%. The background Terra/MODIS satellite image is taken from NASA Worldview (2023).

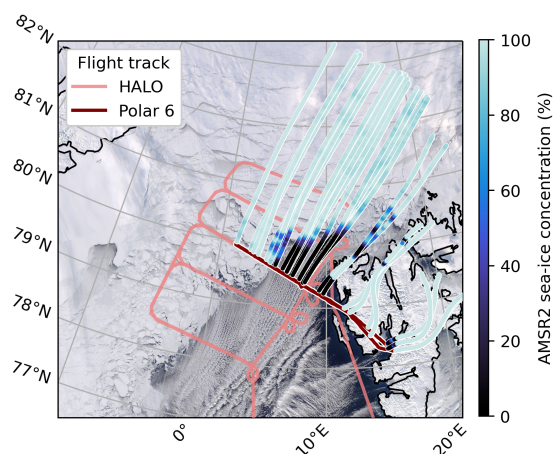


Figure S2. Procedure of calculating the time over ice-free ocean for Polar 6. Air masses are started every 1 min at the flight level. Trajectories are then calculated 12h backwards and the AMSR2 sea-ice concentration (SIC; Ludwig et al., 2020) traced. Time is integrated backwards as long as the SIC is below 20%. The background Terra/MODIS satellite image is taken from NASA Worldview (2023).

Comparison of wind fields from observations, ERA5, and CARRA

5

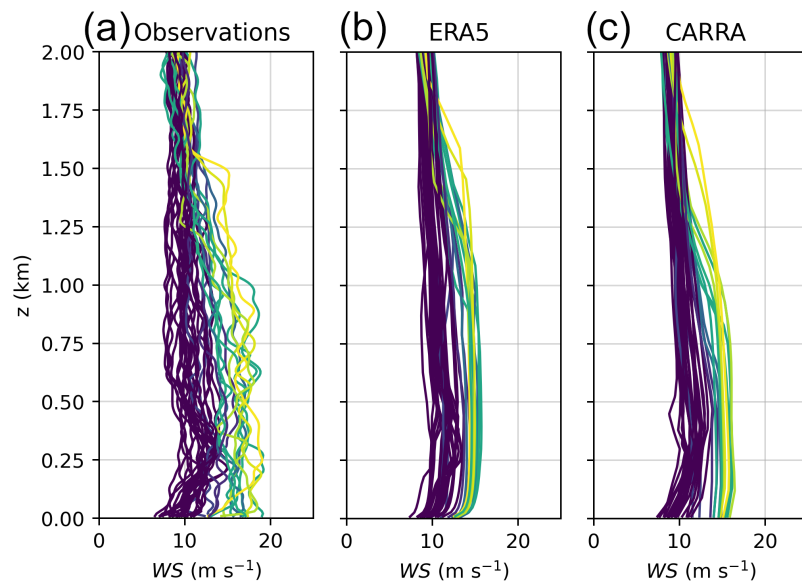


Figure S3. Vertical profiles of wind speed (WS) taken from a) Observations, b) ERA5, and c) CARRA. All profiles are colored by time air masses spent over ice-free ocean before reaching the dropsonde locations.

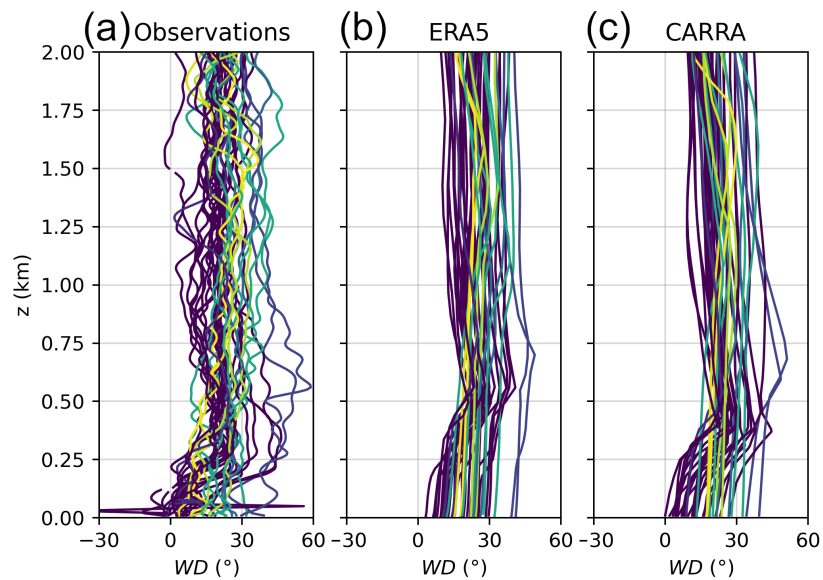


Figure S4. Vertical profiles of wind direction (WD) taken from a) Observations, b) ERA5, and c) CARRA. All profiles are colored by time air masses spent over ice-free ocean before reaching the dropsonde locations.

Investigation of possible cloud-top cooling

The diabatic heating rates not only from observations, but also both ERA5 and CARRA showed altitude ranges where negative values were found, i.e., a net cooling. As these altitudes coincided with the deepening atmospheric boundary layer heights as well as the correlated increasing cloud top heights, it seemed possible that this net diabatic cooling could be a sign of cloud-top radiative cooling. To test this hypothesis, ERA5 temperature tendencies were analyzed, similar as done by others (You et al., 2021a, b; Kirbus et al., 2023a, b). For this purpose, the temperature tendency due to all processes as well as only by terrestrial radiation were evaluated as function of time air masses spent over open ocean. The result is shown in Figure S5. With increasing time over ice-free ocean, stronger negative diabatic heating rates are found at altitudes close to the BLH (Figure S5a). Yet the air masses don't reside long enough at cloud top to actually experience a significant, net cloud top cooling due to radiative processes (Figure S5b). Instead, a vertical turbulent mixing of lower, colder air with the warmer air aloft seems more likely.

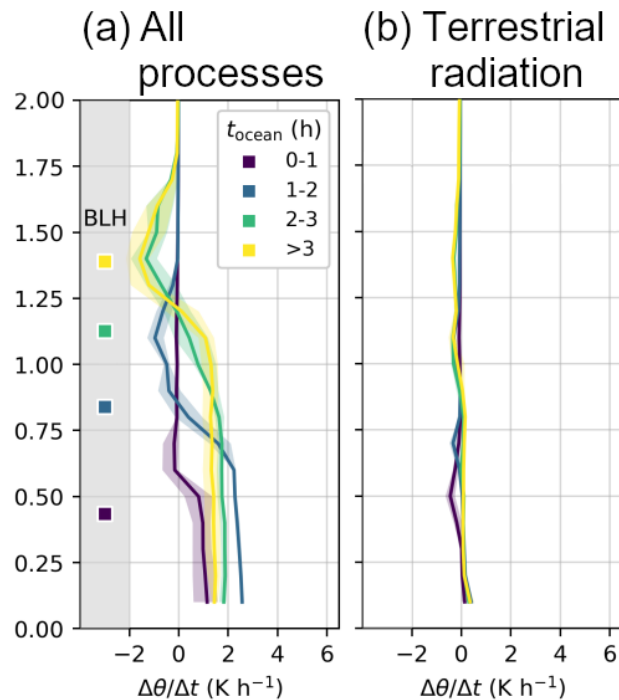


Figure S5. Investigation of suspected cloud top cooling. a) Vertical profile of the ERA5 temperature tendency due to all processes, grouped by time air mass spent over open ocean. b) ERA5 temperature tendency due to terrestrial radiation.

Individual parameters shaping SSHF and SLHF

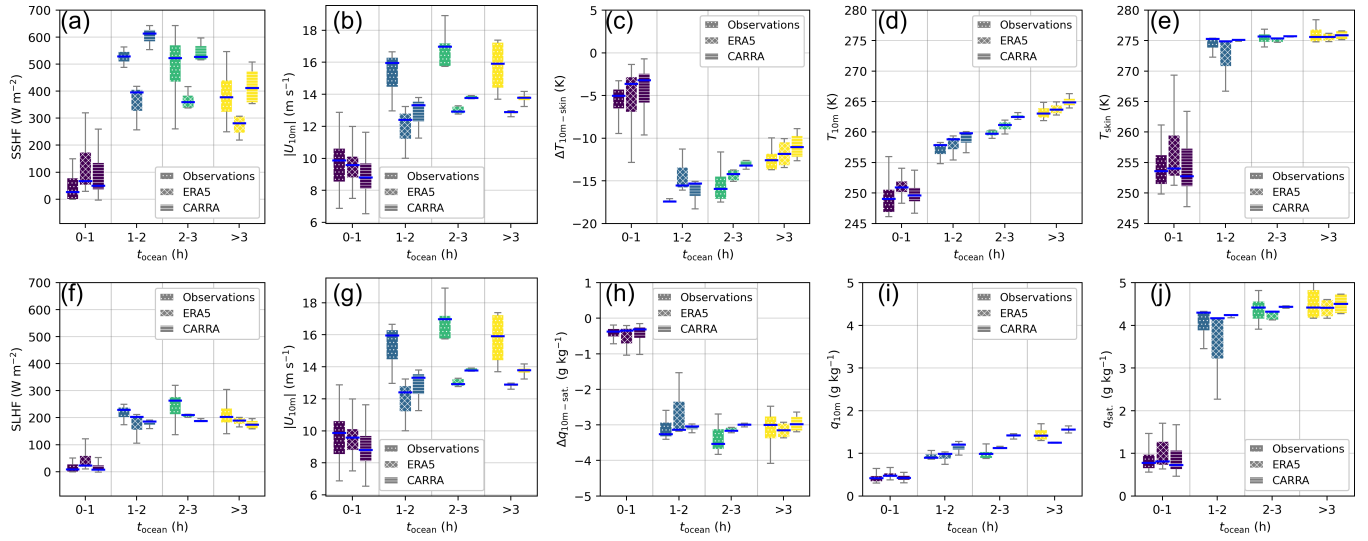


Figure S6. Investigation of the different parameters driving surface sensible heat flux (SSHF, panels a-e) and surface latent heat flux (SLHF, panels f-j). In all panels, data is grouped by the time air masses spent over ice-free ocean, and for observations, ERA5, and CARRA. a) SSHF, b) 10 m wind speed U_{10m} , c) temperature difference between 10-m air temperature T_{10m} and skin temperature T_{skin} , d) T_{10m} , e) T_{skin} . f) SLHF, g) U_{10m} , h) specific humidity difference between 10-m specific humidity q_{10m} and saturation specific humidity taken at sea-surface temperature q_{sat} , i) q_{10m} , j) q_{sat} .

Cloud ice and snow water contents

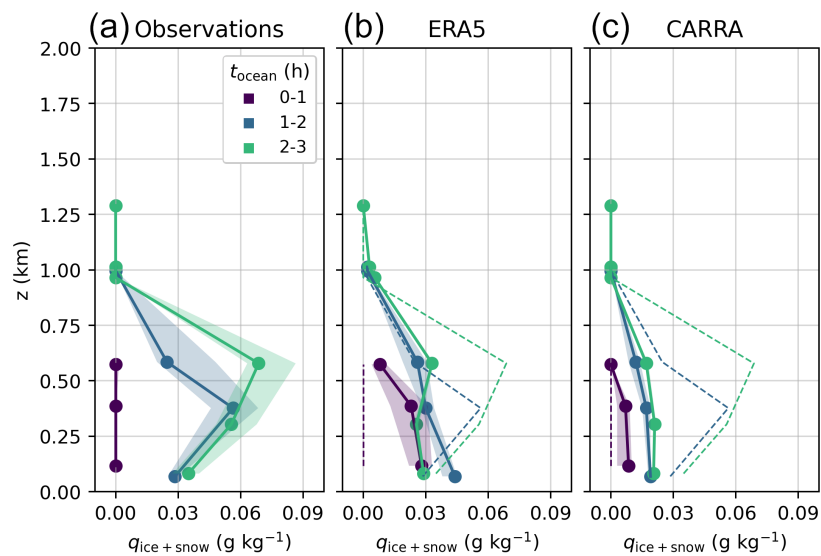


Figure S7. Vertical profiles of cloud frozen (ice and snow) water content, grouped by time air masses spent over ice-free ocean. a) Observations from a Nevzorov sonde aboard Polar 6, b) taken from ERA5, with the observed values as dashed lines, and c) taken from CARRA, with the observed values as dashed lines

20 Climatological comparison of ERA5 and CARRA

To check whether the findings on the performance of CARRA and ERA5 on the 01 April 2022 in representing CAOs are systematic, the difference between the two reanalyses is investigated on a climatological basis. For all days 1991-2022, the CAO index M_{850hPa} is calculated based on ERA5. It is averaged over the Fram Strait box (75-80°N and 10°W-10°E). Only medium to strong CAOs (CAO index larger than 4K) are retained. For this sub-selection, the surface sensible and latent

25 heat fluxes as well as diverse cloud-related parameters are investigated (Figure S8). Under CAO conditions, CARRA shows systematically higher SSHFs over the MIZ and ice-free ocean, lower SLHFs over all surface types, generally lower cloud liquid water contents and especially over the ice-free ocean, as well as lower surface precipitation over the MIZ and open ocean.

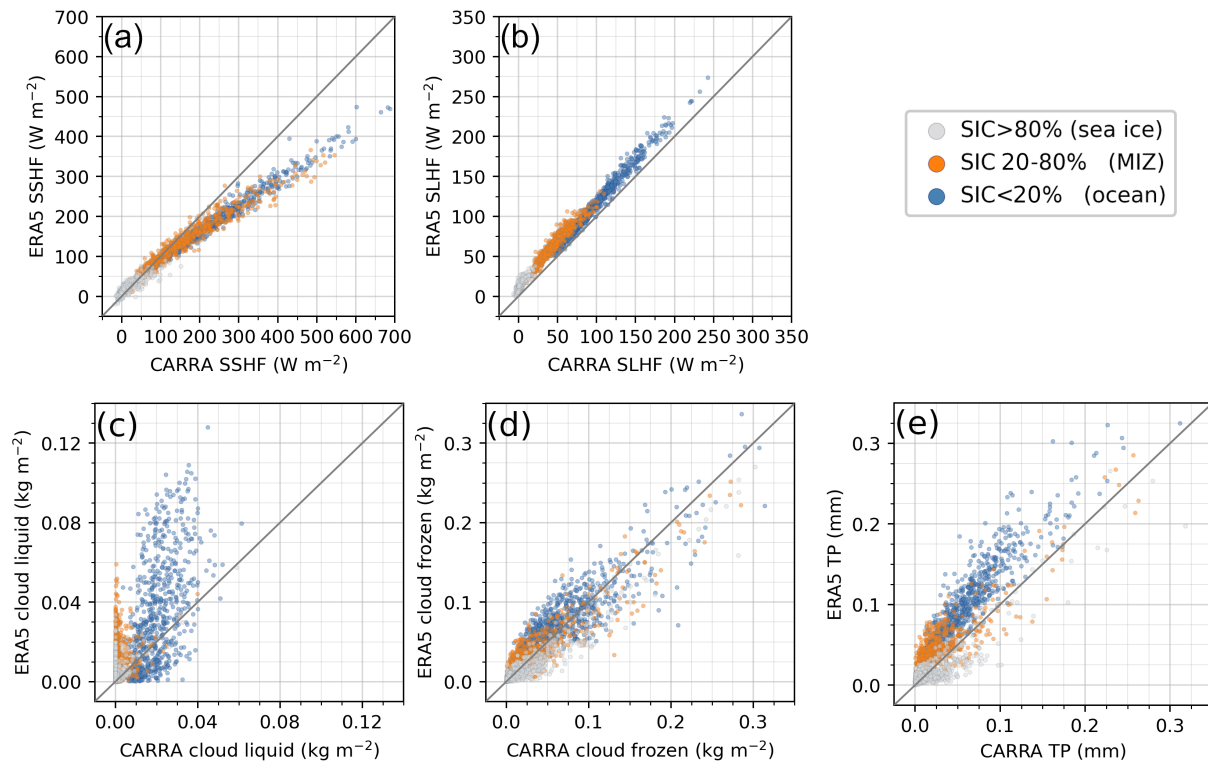


Figure S8. Climatological investigation of differences between CARRA and ERA5 CAOs. All plots depict the daily mean values over the Fram Strait box, separately for sea ice, the MIZ, and ice-free ocean. Panels show the comparisons of a) SSHFs, b) SLHFs, c) total column cloud liquid water content, including rain, d) total column cloud frozen hydrometeors, meaning ice and snow, and e) total precipitation (TP).

References

- Kirbus, B., Chylik, J., Ehrlich, A., Becker, S., Schäfer, M., Neggers, R., and Wendisch, M.: Analysis of an Arctic cold air outbreak during autumn and related air mass transformations forced by surface changes and advection in higher altitudes, *Elem Sci Anth*, 11, <https://doi.org/10.1525/elementa.2023.00079>, 2023a.
- Kirbus, B., Tiedeck, S., Camplani, A., Chylik, J., Crewell, S., Dahlke, S., Ebell, K., Gorodetskaya, I., Griesche, H., Handorf, D., Höschel, I., Lauer, M., Neggers, R., Rückert, J., Shupe, M. D., Spreen, G., Walbröl, A., Wendisch, M., and Rinke, A.: Surface impacts and associated mechanisms of a moisture intrusion into the Arctic observed in mid-April 2020 during MOSAiC, *Front. Earth Sci. Sec. Atmospheric Science*, <https://doi.org/10.3389/feart.2023.1147848>, 2023b.
- Ludwig, V., Spreen, G., and Pedersen, L. T.: Evaluation of a new merged sea-ice concentration dataset at 1 km resolution from thermal infrared and passive microwave satellite data in the Arctic, *Remote Sens. (Basel)*, 12, 3183, 2020.
- NASA Worldview: Corrected Reflectance (True Color) Terra / MODIS, <https://go.nasa.gov/3RMnI48>, (last access: 14 November 2023), 2023.
- You, C., Tjernström, M., and Devasthale, A.: Warm-Air Advection Over Melting Sea-Ice: A Lagrangian Case Study, *Boundary-Layer Meteorology*, 179, 99 – 116, <https://doi.org/10.1007/s10546-020-00590-1>, 2021a.
- You, C., Tjernström, M., and Devasthale, A.: Eulerian and Lagrangian views of warm and moist air intrusions into summer Arctic, *Atmospheric Research*, 256, 105 586, <https://doi.org/10.1016/j.atmosres.2021.105586>, 2021b.